



Contents lists available at ScienceDirect

Tunnelling and Underground Space Technology incorporating Trenchless Technology Research

journal homepage: www.elsevier.com/locate/tust

Advancements in smoke control strategies for metro tunnel cross-passage: A theoretical and numerical study on critical velocity and driving force

Zhihe Su^a, Yanfeng Li^{a,*}, Hua Zhong^{b,*}, Junmei Li^a, Zhicheng Guo^a, Xin Yang^a, Shi Yang^a^a Beijing Key Laboratory of Green Built Environment and Energy Efficient Technology, Beijing University of Technology Beijing, China^b School of the Built Environment and Architecture, London South Bank University, 103 Borough Road, London SE1 0AA, United Kingdom

ARTICLE INFO

Keywords:

Metro tunnel fire
Critical velocity
Tunnel cross-passage
Required pressure
Fan selection

ABSTRACT

Cross-passage is a commonly encountered structure within metro tunnels, providing a swift route for evacuating personnel from the accident tunnel to the safe tunnel opposite. Ventilation in the cross-passage of metro tunnels is established through the collaborative operation of ventilation systems on both sides of the tunnel. Concurrently, smoke movement within the metro tunnel is impacted by factors such as train blockage and the accumulation of heat within the train carriages. The former correlations need further refinement to predict the critical velocity and driving force required to prevent smoke from spreading into a metro tunnel cross-passage. One-dimensional theoretical analysis and full-scale cold smoke experiments were performed to investigate the relationship between the air supply parameters of tunnel fans on both sides and the ventilation velocity in the cross-passage. A calculation model of fan type selection in the opposite side safe tunnel for smoke control in the tunnel cross-passage is proposed. The influence of train location, fire heat release rate, and main tunnel ventilation velocity on critical velocity in the cross-passage was quantified by numerical simulations. The results show that the critical velocity in the cross-passage under unobstructed conditions surpasses that under blocked conditions. Meanwhile, the critical velocity exhibits relative stability under both unobstructed and blocked conditions. On the basis of the dimensionless analysis, a piecewise function was proposed to predict the critical velocity in tunnel cross-passage. The outcomes of this study provide valuable guidance for the implementation of fire prevention and smoke control measures in tunnels with similar structures.

1. Introduction

Tunnel fires can pose a substantial threat to the safety of passengers and firefighters. Especially in metro tunnels, the difficulty of evacuating during fire incidents is heightened due to the double-long and narrow structure (Cong et al., 2020; Zhang et al., 2016). Compared with the flames themselves, the existence of toxic gases and smoke particles often leads to greater casualties (Lu et al., 2022; Tang et al., 2013). Especially in tunnels with long intervals, evacuation options are confined to tunnel exits and cross-passages, consequently amplifying evacuation risks. Therefore, ensuring effective prevention of smoke transportation into cross-passages is imperative to guarantee a safe evacuation process.

The critical velocity, which denotes the minimum velocity necessary to prevent smoke from flowing backwards, plays a crucial role in creating a secure environment for both evacuation and firefighting. This aspect has been extensively investigated by many researchers (Li et al., 2010; Thomas, 1958; Wu and Bakar, 2000). The majority of research on

the critical velocity of single tunnels focuses on tunnel slope (Gao et al., 2022; Jiang and Xiao, 2022; Weng et al., 2016) and cross-section (Li and Ingason, 2017). For different fire scenarios, some scholars have focused on the effect of train blockage on critical velocity (Hu et al., 2020; Su et al., 2023; Weng et al., 2015; Zhang et al., 2016; Zhao et al., 2018). In recent years, some scholars have been devoted to the study of critical velocity in tunnels with bifurcated structures. Huang et al. (2020) theoretically analyzed the critical velocity and required driving force in a branched tunnel fire. The fire source and bifurcation angle were considered, and a predicted critical velocity model was proposed based on the theoretical analysis of pressure change. Chen et al. (2023a) experimentally researched the influence of longitudinal fire location on the critical velocity for a fire scenario in a T-shaped split tunnel with longitudinal ventilation in the main tunnel. An empirical correlation of the critical velocity was proposed on the basis of the proportionality coefficient k_l/k_e .

Tunnel cross-passage connects the main tunnel to a safe place, and provides a safe route for evacuation and rescue operations. Previous

* Corresponding authors at: Beijing University of Technology, Beijing 100124, China.

E-mail addresses: liyanfeng@bjut.edu.cn, 2848765191@qq.com (Y. Li), hua.zhong@lsbu.ac.uk (H. Zhong).

<https://doi.org/10.1016/j.tust.2024.105734>

Received 11 October 2023; Received in revised form 4 February 2024; Accepted 27 March 2024

Available online 1 April 2024

0886-7798/© 2024 The Authors. Published by Elsevier Ltd. This is an open access article under the CC BY license (<http://creativecommons.org/licenses/by/4.0/>).

Nomenclature			
Q	Heat release rate (kW)	D_t	Hydraulic diameter of the tunnel (m)
Q^*	Dimensionless heat release rate	D_c	Hydraulic diameter of the cross-passage (m)
c_p	Thermal heat capacity of air (J/(kg·K))	T_0	Ambient temperature (K)
ΔP_{fire}	Pressure loss induced by the fire (Pa)	V_s	Longitudinal velocity of smoke (m/s)
ΔP_λ	Pressure loss due to tunnel and train wall friction (Pa)	V_{cc}	Critical velocity in the tunnel cross-passage (m/s)
ΔP_ζ	Pressure loss due to local flow resistance (Pa)	A_t	Cross-sectional area of the main tunnel (m ²)
V_c	Critical velocity in the main tunnel (m/s)	<i>Greek letters</i>	
ζ_{fire}	Coefficient of pressure loss caused by the fire plume blockage and air viscosity	ρ_∞	Ambient density (kg/m ³)
q_s	Volume of wind and smoke mixed together in the main tunnel (m ³ /s)	λ	Wall friction coefficient
X	Fire location	ζ	Local resistance coefficient
V_t	Main tunnel ventilation velocity (m/s)	<i>Superscript and subscript</i>	
q_{cc}	Wind volume of the tunnel cross-passage (m ³ /s)	*	Dimensionless expression
q_{out}	Total volume downstream of the left tunnel (m ³ /s)	cross	Cross-passage
A_{cross}	Cross-sectional area of the cross-passage (m ²)	in	Portal
		out	Exit
		t	Tunnel

studies have focused on preventing smoke from spreading into a cross-passage to provide a safe route for evacuation and rescue operations. Li et al. (2013) investigated factors influencing the critical velocity to prevent smoke flow in a tunnel cross-passage, considering the fireproof door, heat release rate, and ventilation speed. A dimensionless correlation was proposed to calculate the critical velocity in the tunnel cross-passage based on the dimensional analysis. Chen et al., (2023b) conducted a 1/10 model-scaled tunnel with an inclined cross-passage to analyze the effect mechanism of the cross-passage slope and deduced the dimensionless critical velocity under different cross-passage slopes. For the impact of the cross-passage on the smoke spread in the main tunnel. Yao et al. (2023) numerically studied the influence of heat release rates, fire locations, longitudinal ventilation velocities, and cross-passage intervals on the smoke movement and control in longitudinal ventilated tunnel fires with cross-passages, and a smoke back-layering length prediction model in the main tunnel considering the fire position and interval of cross-passages was proposed.

Metro tunnels are frequently subject to train blockage. Simultaneously, in the event of a fire, the conformation of trains and tunnels creates a double long and narrow space, resulting in the accumulation of a substantial volume of smoke and heat within the train carriages. Concerning smoke control in the cross-passage of metro tunnels, for instance, Liu et al. (2020) experimentally and numerically studied the critical velocity in metro connect tunnels, considering the inclination of connected tunnels and the incorporation of longitudinal ventilation in a main tunnel. A prediction model of the critical velocity for confining smoke in metro-connected tunnels was developed. However, the effect of train blocking on smoke movement was not considered. Feng et al. (2020) analyzed the influence of tunnel shape, fire location, and train blocking on critical velocity in the metro tunnel cross-passage. However, the combined effects of airflow pressure and velocity from both sides of the tunnels on the airflow within the cross-passage have not been taken into consideration. Additionally, the critical velocity required within the cross-passage during train blockage remains yet to be determined. Li et al. (2012) conducted both theoretical and experimental investigations to examine the impact of heat release rate (HRR), train obstruction, fire source location, ventilation conditions, and the open height below blocks on smoke control in cross-passages within a rescue station. The findings indicate that the presence of a train causes a decrease in critical velocity, and the average critical velocity ratio due to obstruction is approximately 0.86. Nevertheless, a critical aspect is the presence of jet fans installed in the cross-passage of the ordinary tunnel, contrasting with the metro tunnel, where the airflow in the metro tunnel cross-passage is obtained based on the joint operation of systems on both

sides of the tunnel. The cross-passage in metro tunnel inherently lacks the capability to actively maintain a constant air velocity. The disparate airflow parameters in the two adjacent tunnels result in a pressure differential along the cross-passage, inducing the inflow of fresh air.

The purpose of fireproof doors in the cross-passage is to prevent the spread of smoke from the accident tunnel to the opposite safe tunnel. However, the fireproof doors in the cross-passage between the two tracks of the subway are subjected to prolonged reciprocating forces from the piston-driven air pressure generated by passing trains. This has led to instances of damage and detachment, posing a threat to the safety of train operations. At the same time, it is essential to initiate the longitudinal ventilation system within the accident tunnel during a fire incident. This action induces a specific pressure differential between the two side tunnels, facilitating the inflow of fresh air into the cross-passage and acting as a preventive measure to impede the dissemination of smoke towards the opposite safety tunnel. Hence, it is imperative to deliberate on strategies for harnessing the inflow of fresh air into the cross-passage to prevent the dispersion of smoke towards the opposite tunnel, as an alternative to the installation of fireproof doors. This approach aims to address the operational safety risks associated with the presence of fire doors.

This study aimed to analyze the relationship between the ventilation parameters of tunnel fans on both sides and the ventilation velocity in the cross-passage. Simultaneously, the effects of train location, fire heat release rate, and longitudinal ventilation velocity on the critical velocity in the metro tunnel cross-passage are quantified to provide theoretical guidance for cancelling fireproof doors in cross-passage in the future. The research outcome can provide technical guidance on the ventilation design and evacuation process during an emergency train fire in a metro tunnel.

2. Theoretical model

In fact, there is no active ventilation system within the metro tunnel cross-passage, and the ventilation velocity within the cross-passage is intricately linked to the pressure differential between the two side tunnels. In the event of a metro tunnel fire, the opposite side safe tunnel will similarly employ ventilation systems to generate an appropriate positive pressure at the cross-passage. Fig. 1 illustrates a schematic diagram depicting the air supply system in both the accident tunnel and the safe tunnel on the opposite side. In order to establish the relationship between the supply parameters of the tunnel fans on both sides and the ventilation velocity within the cross-passage, the tunnel was divided into two segments for analysis, namely, from portal A and C to exit B,

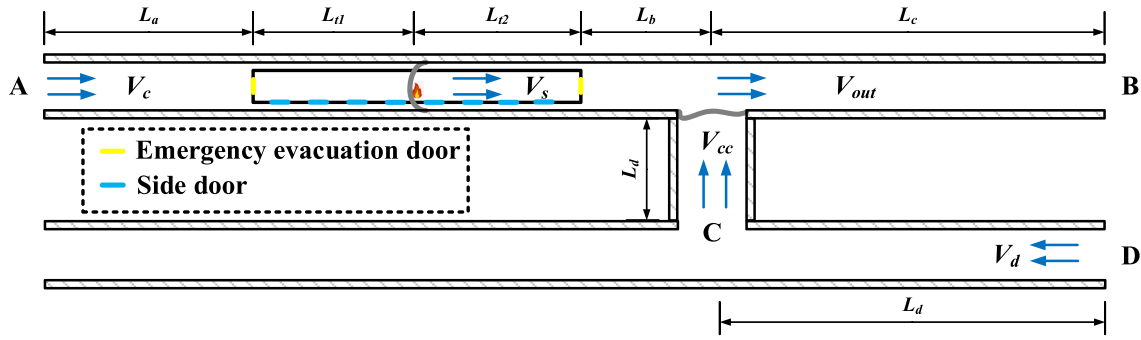


Fig. 1. Schematic diagram depicting the air supply system in both side tunnels.

and from portal D to portal C.

2.1. Driving force required at portal C for a train stopped in front of the cross-passage

Compared with the single tunnel, there are two critical velocities for metro train stopped in the tunnel with cross-passage. The first is that the smoke would not spread upwards in the mainline tunnel under enough forced critical velocity. Secondly, the smoke would not spread into the cross-passage after shunting. The tunnel portal, exit and cross-passage portal are indicated by the symbols A, B, and C in Fig. 2. The schematic diagram illustrating smoke movement for train stopped in front of the cross-passage under critical velocity conditions is presented in Fig. 2 (a). The total pressure loss ΔP within the metro tunnel with cross-passage during a fire under forced ventilation can be described by Eq. (1):

$$\Delta P = \Delta P_{\text{fire}} + \Delta P_{\lambda} + \Delta P_{\zeta} \tag{1}$$

where ΔP_{fire} is the pressure loss induced by the fire in Pa, ΔP_{λ} is the pressure loss due to tunnel and train wall friction in Pa, ΔP_{ζ} is the

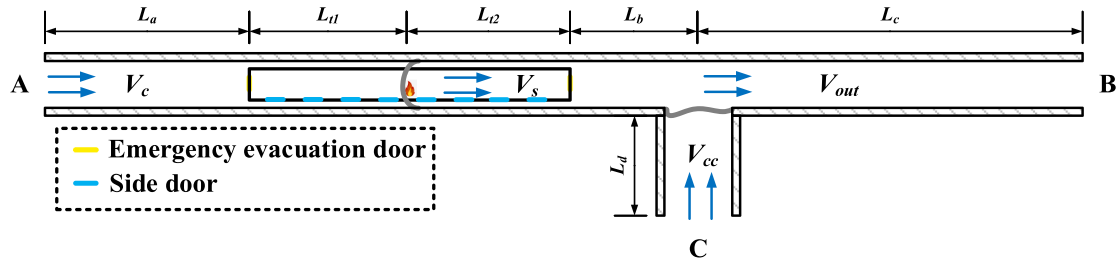
pressure loss due to local flow resistance in Pa.

(1) Pressure losses induced by the fire source

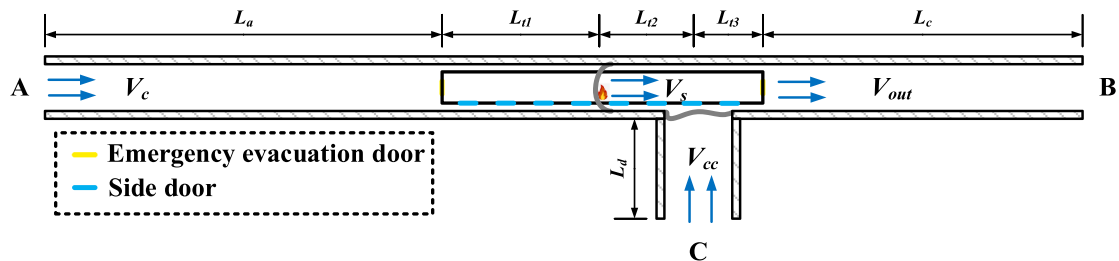
In this study, the emergency evacuation doors and side doors are configured to be in the open position, indicating the emergency evacuation scenario when the metro comes to a stop within the tunnel. Therefore, during the longitudinal ventilation flow through the metro carriages, it can be approximately assumed that the velocity remains consistent across the entire tunnel cross-section. The pressure loss induced by the fire source is composed of two parts which are thermal resistance and airflow local resistance. Ignore the thickness of the train carriage, the pressure loss induced by the fire source in the metro carriage can be estimated according to the following equation (Du et al., 2018):

$$\Delta P_{\text{fire}} = \frac{1}{2} \frac{\dot{Q} V_c}{c_p A_t T_{\infty}} + \frac{1}{2} \zeta_{\text{fire}} \rho_{\infty} V_c^2 \tag{2}$$

where A_t is the cross-sectional area of the main tunnel, ζ_{fire} is the coefficient of pressure loss caused by the fire plume blockage and air viscosity, V_c is the critical velocity in the main tunnel. Previous study has shown that local pressure loss accounts for up to 4 % of ventilation



(a)



(b)

Fig. 2. Schematic diagram of smoke movement under the critical velocity condition: (a) The train stopped in front of the cross-passage, (b) The train stopped near the cross-passage.

resistance (Yao et al., 2022). Therefore, the Eq. (2) can be simplified as follows:

$$\Delta P_{\text{fire}} = \frac{1}{2} \frac{\dot{Q} V_c}{c_p A_t T_\infty} \quad (3)$$

(2) Pressure losses induced by the tunnel and train wall friction

The pressure losses caused by wall friction can be divided into two parts: the pressure loss caused by the tunnel wall friction ($L_a + L_b + L_c + L_d$) and the pressure losses caused by the joint action of the tunnel and train wall friction ($L_{t1} + L_{t2}$). Assuming that the flow velocity on the cross-section is uniformly distributed. The mass continuity equation is expressed as follows:

$$m_s + m_{cc} = m_{out} \quad (4)$$

where m_s is the mass flow rate of wind and smoke mixed together in the main tunnel, m_{cc} is the mass flow rate of the tunnel cross-passage, and m_{out} is the total mass flow rate downstream of the left tunnel. Subsequently, based on the principle of conservation of mass, the total velocity downstream of the left tunnel can be derived as:

$$\rho_s V_s A_t + \rho_\infty V_{cc} A_{cross} = \rho_{out} V_{out} A_t \quad (5)$$

$$V_{out} = \frac{\rho_s}{\rho_{out}} V_s + \frac{\rho_\infty}{\rho_{out}} \frac{A_{cross}}{A_t} V_{cc} \quad (6)$$

where A_{cross} is the cross-sectional area of the cross-passage, V_{cc} is the critical velocity in the tunnel cross-passage, V_s is the longitudinal velocity of smoke, ρ_s is the density of smoke. Subsequently, the pressure losses induced by the tunnel and train wall friction can be estimated by the following (Du et al., 2018).

The pressure losses induced by the tunnel and train wall friction from entrance A to exit B is expressed as:

$$\Delta P_\lambda = \lambda \frac{1}{2} \frac{L_a}{D_t} \rho_\infty V_c^2 + \lambda_{\text{train}} \frac{1}{2} \frac{L_{t1}}{D_t} \rho_\infty V_c^2 + \lambda_{\text{train}} \frac{1}{2} \frac{L_{t2}}{D_t} \rho_s V_s^2 + \lambda \frac{1}{2} \frac{L_b}{D_t} \rho_s V_s^2 + \lambda \frac{1}{2} \frac{L_c}{D_t} \rho_s V_{out}^2 \quad (7a)$$

The pressure losses induced by the tunnel wall friction from entrance C to exit B is expressed as:

$$\Delta P_\lambda = \lambda \frac{1}{2} \frac{L_d}{D_c} \rho_\infty V_{cc}^2 + \lambda \frac{1}{2} \frac{L_c}{D_t} \rho_s V_{out}^2 \quad (7b)$$

where λ is the friction coefficient of the tunnel, λ_{train} is the friction coefficient under the combined influence of the tunnel and the train, D_t is the hydraulic diameter of the tunnel, D_c is the hydraulic diameter of the cross-passage.

Due to thermal expansion, the acceleration of longitudinal flow occurs after the airflow passes through the fire zone. Assuming that the flow is inviscid, the pressure losses due to thermal expansion ΔP_t can be represented by the following equation based on the momentum conservation equation.

$$\Delta P_t = \frac{1}{2} \rho_s V_s^2 - \frac{1}{2} \rho_\infty V_c^2 \quad (8)$$

The mass flow rate generated by combustion is significantly lower than the upstream mass flow rate of air (Yao et al., 2022). Assuming a constant mass flow rate in the tunnel, Eq. (9) is derived from the mass conservation equation. At the same time, combined with the ideal gas law and conservation equation, the longitudinal velocity of smoke can be expressed as Eq. (10). Assuming that the hypothesis of gas constant R_s and R_∞ are the same. Therefore, Eq. (10) can be transferred into Eq. (11)

(Du et al., 2018).

$$\rho_s V_s = \rho_\infty V_c \quad (9)$$

$$V_s = \frac{\rho_\infty V_c}{\rho_s} = \frac{R_s T_s}{R_\infty T_\infty} V_c = \frac{R_s \left(T_\infty + \frac{\dot{Q}}{C_p \rho_\infty V_c A_t} \right)}{R_\infty T_\infty} V_c \quad (10)$$

$$V_s = V_c + \frac{\dot{Q}}{C_p \rho_\infty A_t T_\infty} \quad (11)$$

Substituting Eqs. (9), (11) into Eq. (7), the pressure losses induced by the tunnel and train wall friction can be obtained.

The pressure losses induced by the tunnel and train wall friction from entrance A to exit B is expressed as:

$$\Delta P_\lambda = \lambda \frac{1}{2} \frac{(L_a + L_b)}{D_t} \rho_\infty V_c^2 + \lambda_{\text{train}} \frac{1}{2} \frac{(L_{t1} + L_{t2})}{D_t} \rho_\infty V_c^2 + \lambda_{\text{train}} \frac{1}{2} \frac{L_{t2}}{D_t} \rho_\infty \frac{\dot{Q} V_c}{C_p \rho_\infty A_t T_\infty} + \lambda \frac{1}{2} \frac{L_b}{D_t} \rho_\infty \frac{\dot{Q} V_c}{C_p \rho_\infty A_t T_\infty} + \lambda \frac{1}{2} \frac{L_c}{D_t} \frac{\rho_\infty V_c}{V_c + \frac{\dot{Q}}{C_p \rho_\infty A_t T_\infty}} V_{out}^2 \quad (12a)$$

The pressure losses induced by the tunnel wall friction from entrance C to exit B is expressed as:

$$\Delta P_\lambda = \lambda \frac{1}{2} \frac{L_d}{D_c} \rho_\infty V_{cc}^2 + \lambda \frac{1}{2} \frac{L_c}{D_t} \frac{\rho_\infty V_c}{V_c + \frac{\dot{Q}}{C_p \rho_\infty A_t T_\infty}} V_{out}^2 \quad (12b)$$

(3) Pressure losses induced by the local flow resistance

The pressure losses induced by the local flow resistance in current scenario includes the resistance at tunnel portal, combining point, train portal, train exit, cross-passage portal and tunnel exit.

The pressure losses induced by the local flow resistance in the metro tunnel from entrance A to exit B is expressed as:

$$\Delta P_\zeta = \zeta_{in-A} \frac{\rho_\infty V_c^2}{2} + \zeta_{in-train} \frac{\rho_\infty V_c^2}{2} + \zeta_{out-train} \frac{\rho_s V_s^2}{2} + \zeta_{A-B} \frac{\rho_s V_s^2}{2} + \zeta_{out-B} \frac{\rho_s V_{out}^2}{2} \quad (13a)$$

The pressure losses induced by the local flow resistance in the metro tunnel from entrance C to exit B is expressed as:

$$\Delta P_\zeta = \zeta_{in-C} \frac{\rho_\infty V_{cc}^2}{2} + \zeta_{C-B} \frac{\rho_\infty V_{cc}^2}{2} + \zeta_{out-B} \frac{\rho_s V_{out}^2}{2} \quad (13b)$$

where ζ_{in-A} and ζ_{in-C} are the local resistance coefficient of the tunnel and cross-passage portal, which are 0.5. ζ_{out-B} is the local resistance coefficient of the tunnel exit, which is 1.0. $\zeta_{in-train}$ and $\zeta_{out-train}$ are the local resistance coefficient of the train front and train rear, which are needed to be determined in the following. ζ_{A-B} and ζ_{C-B} are the local resistance coefficient of combining flow from tunnel A to tunnel B and cross-passage C and tunnel B. The local resistance coefficient caused by airflow combination are related to the cross-sectional areas and the ratio of the flow rate, which can be calculated by following equations (Hager, 2010).

$$\zeta_{A-B} = q_\delta (2 - q_\delta) \quad (14a)$$

$$\zeta_{C-B} = q_\delta^2 \left(\left(\frac{A_t}{A_{cross}} \right)^2 - 2 \right) + 4q_\delta - 1 \quad (14b)$$

where $q_\delta = (A_{cross} V_{cc}) / [A_t (V_{cc} + V_s)]$ is the flow rate ratio between cross-passage q_{cross} and main tunnel q_t , A_{cross} is the cross-sectional area

of the cross-passage. Substituting Eqs. (9), (11) and (14) into Eq. (13), the pressure losses induced by the local flow resistance can be obtained.

The pressure losses induced by the local flow resistance in the metro tunnel from entrance A to exit B is expressed as:

$$\Delta P_{\zeta} = (\zeta_{in-A} + \zeta_{in-train} + \zeta_{out-train} + q_{\delta}(2 - q_{\delta})) \frac{\rho_{\infty} V_c^2}{2} + (\zeta_{out-train} + q_{\delta}(2 - q_{\delta})) \frac{\rho_{\infty}}{2} \frac{\dot{Q} V_c}{C_p \rho_{\infty} A_t T_{\infty}} + \zeta_{out-B} \frac{\rho_{\infty} V_c}{2 \left(V_c + \frac{\dot{Q}}{C_p \rho_{\infty} A_t T_{\infty}} \right)} V_{out}^2 \quad (15a)$$

The pressure losses induced by the local flow resistance in the metro tunnel from entrance C to exit B is expressed as:

$$\Delta P_{\zeta} = \zeta_{in-C} \frac{\rho_{\infty} V_{cc}^2}{2} + \left(q_{\delta}^2 \left(\left(\frac{A_t}{A_{cross}} \right)^2 - 2 \right) + 4q_{\delta} - 1 \right) \frac{\rho_{\infty} V_c}{2 \left(V_c + \frac{\dot{Q}}{C_p \rho_{\infty} A_t T_{\infty}} \right)} V_{out}^2 \quad (15b)$$

Substituting Eq. (3), (12) and (15) into Eq. (1), the simplified model of the driving force for fire in a metro tunnel with cross-passage during a fire under forced ventilation can be described as follows:

The pressure losses in the metro tunnel from entrance A to exit B is expressed as:

$$\begin{aligned} \Delta P_{A-B} &= P_A - P_B \\ &= \frac{1}{2} \frac{\dot{Q} V_c}{c_p A_t T_{\infty}} + \lambda \frac{1}{2} \frac{(L_a + L_b)}{D_t} \rho_{\infty} V_c^2 + \lambda_{train} \frac{1}{2} \frac{(L_{t1} + L_{t2})}{D_t} \rho_{\infty} V_c^2 + \lambda_{train} \frac{1}{2} \frac{L_{t2}}{D_t} \rho_{\infty} \frac{\dot{Q} V_c}{C_p \rho_{\infty} A_t T_{\infty}} \\ &+ \lambda \frac{1}{2} \frac{L_b}{D_t} \rho_{\infty} \frac{\dot{Q} V_c}{C_p \rho_{\infty} A_t T_{\infty}} + \lambda \frac{1}{2} \frac{L_c}{D_t} \frac{\rho_{\infty} V_c}{V_c + \frac{\dot{Q}}{C_p \rho_{\infty} A_t T_{\infty}}} V_{out}^2 + (\zeta_{in-A} + \zeta_{in-train} + \zeta_{out-train} + q_{\delta}(2 - q_{\delta})) \frac{\rho_{\infty} V_c^2}{2} \\ &+ \zeta_{out-B} \frac{\rho_{\infty} V_c}{2 \left(V_c + \frac{\dot{Q}}{C_p \rho_{\infty} A_t T_{\infty}} \right)} V_{out}^2 + (\zeta_{out-train} + q_{\delta}(2 - q_{\delta})) \frac{\rho_{\infty}}{2} \frac{\dot{Q} V_c}{C_p \rho_{\infty} A_t T_{\infty}} \end{aligned} \quad (16a)$$

$$\begin{aligned} P_C &= P_A + \left(\zeta_{in-C} + q_{\delta}^2 \left(\left(\frac{A_t}{A_{cross}} \right)^2 - 2 \right) + 4q_{\delta} - 1 \right) \frac{\rho_{\infty} V_{cc}^2}{2} + \lambda \frac{1}{2} \frac{L_d}{D_c} \rho_{\infty} V_{cc}^2 - \lambda \frac{1}{2} \frac{L_b}{D_t} \rho_{\infty} \frac{\dot{Q} V_c}{c_p \rho_{\infty} D_t T_{\infty}} \\ &- \frac{1}{2} \frac{\dot{Q} V_c}{c_p A_t T_{\infty}} - \lambda \frac{1}{2} \frac{(L_a + L_b)}{D_t} \rho_{\infty} V_c^2 - \lambda_{train} \frac{1}{2} \frac{(L_{t1} + L_{t2})}{D_t} \rho_{\infty} V_c^2 - \lambda_{train} \frac{1}{2} \frac{L_{t2}}{D_t} \rho_{\infty} \frac{\dot{Q} V_c}{c_p \rho_{\infty} D_t T_{\infty}} \\ &- [\zeta_{in-A} + \zeta_{in-train} + \zeta_{out-train} + q_{\delta}(2 - q_{\delta})] \frac{\rho_{\infty} V_c^2}{2} - [q_{\delta}(2 - q_{\delta}) + \zeta_{out-train}] \frac{\rho_{\infty}}{2} \frac{\dot{Q} V_c}{C_p \rho_{\infty} D_t T_{\infty}} \end{aligned} \quad (17)$$

The pressure losses in the metro tunnel from entrance C to exit B is expressed as:

$$\begin{aligned} \Delta P_{C-B} &= P_C - P_B \\ &= \lambda \frac{1}{2} \frac{L_d}{D_c} \rho_{\infty} V_{cc}^2 + \lambda \frac{1}{2} \frac{L_c}{D_t} \frac{\rho_{\infty} V_c}{V_c + \frac{\dot{Q}}{C_p \rho_{\infty} A_t T_{\infty}}} V_{out}^2 + \zeta_{out-B} \frac{\rho_{\infty} V_c}{2 \left(V_c + \frac{\dot{Q}}{C_p \rho_{\infty} A_t T_{\infty}} \right)} V_{out}^2 \\ &+ \zeta_{in-C} \frac{\rho_{\infty} V_{cc}^2}{2} + \left(q_{\delta}^2 \left(\left(\frac{A_t}{A_{cross}} \right)^2 - 2 \right) + 4q_{\delta} - 1 \right) \frac{\rho_{\infty} V_c^2}{2} \end{aligned} \quad (16b)$$

Thus, the required driving force at entrance C under critical conditions can be expressed as:

2.2. Driving force required at portal C for a train stopped near the cross-passage

The smoke movement schematic in a metro tunnel cross-passage for

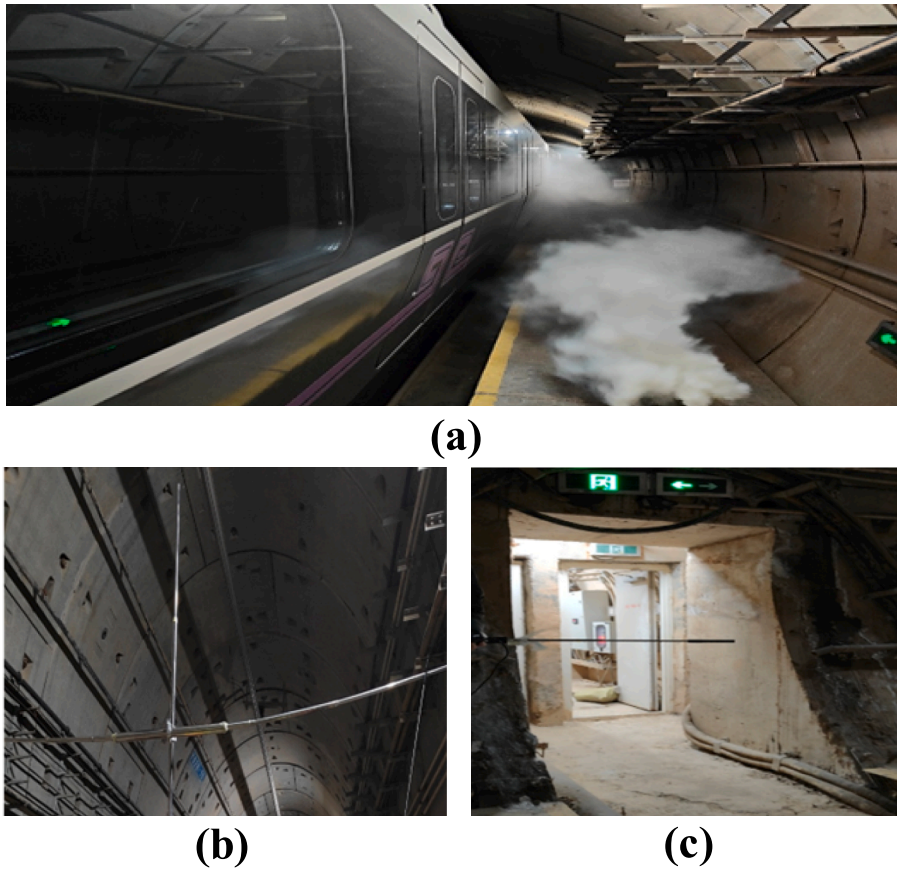


Fig. 3. Schematic diagram of cold smoke experiment: (a) cold smoke, (b) measuring in tunnel, (c) measuring in cross-passage.

the train stopped near the cross-passage is shown in Fig. 2(b). Similarly, the total pressure loss ΔP consists of three parts: the fire source resistance ΔP_{fire} , the frictional resistance ΔP_λ and the local resistance ΔP_ζ . At the same time, the pressure induced by the wall friction and the local flow resistance can be expressed as follows.

The pressure losses induced by the tunnel and train wall friction from entrance A to exit B is expressed as:

$$\Delta P_\lambda = \lambda \frac{1}{2} \frac{L_a}{D_t} \rho_\infty V_t^2 + \lambda_{train} \frac{1}{2} \frac{L_{t1}}{D_t} \rho_\infty V_c^2 + \lambda_{train} \frac{1}{2} \frac{L_{t2}}{D_t} \rho_s V_s^2 + \lambda_{train} \frac{1}{2} \frac{L_{t3}}{D_t} \rho_s V_{out}^2 + \lambda \frac{1}{2} \frac{L_c}{D_t} \rho_s V_{out}^2 \quad (18a)$$

The pressure losses induced by the tunnel wall friction from entrance C to exit B is expressed as:

$$\Delta P_\lambda = \lambda \frac{1}{2} \frac{L_d}{D_c} \rho_\infty V_{cc}^2 + \lambda_{train} \frac{1}{2} \frac{L_{t3}}{D_t} \rho_s V_{out}^2 + \lambda \frac{1}{2} \frac{L_c}{D_t} \rho_s V_{out}^2 \quad (18b)$$

The pressure losses induced by the local flow resistance in the metro

$$P_C = P_A + \left(\zeta_{in-C} + q_\delta^2 \left(\left(\frac{A_t}{A_{cross}} \right)^2 - 2 \right) + 4q_\delta - 1 \right) \frac{\rho_\infty V_{cc}^2}{2} + \lambda \frac{1}{2} \frac{L_d}{D_c} \rho_\infty V_{cc}^2 - \frac{1}{2} \frac{\dot{Q}V_c}{c_p A_t T_\infty} - \lambda \frac{1}{2} \frac{L_a}{D_t} \rho_\infty V_c^2 - \lambda_{train} \frac{1}{2} \frac{(L_{t1} + L_{t2})}{D_t} \rho_\infty V_c^2 - \lambda_{train} \frac{1}{2} \frac{L_{t2}}{D_t} \rho_\infty \frac{\dot{Q}V_c}{c_p \rho_\infty D_t T_\infty} - [\zeta_{in-A} + \zeta_{in-train} + q_\delta(2 - q_\delta)] \frac{\rho_\infty V_c^2}{2} - q_\delta(2 - q_\delta) \frac{\rho_\infty}{2} \frac{\dot{Q}V_c}{c_p \rho_\infty D_t T_\infty} \quad (20)$$

tunnel from entrance A to exit B is expressed as:

$$\Delta P_\zeta = \zeta_{in-A} \frac{\rho_\infty V_c^2}{2} + \zeta_{in-train} \frac{\rho_\infty V_c^2}{2} + \zeta_{A-B} \frac{\rho_s V_s^2}{2} + \zeta_{out-train} \frac{\rho_s V_{out}^2}{2} + \zeta_{out-B} \frac{\rho_s V_{out}^2}{2} \quad (19a)$$

The pressure losses induced by the local flow resistance in the metro tunnel from entrance C to exit B is expressed as:

$$\Delta P_\zeta = \zeta_{in-C} \frac{\rho_\infty V_{cc}^2}{2} + \zeta_{C-B} \frac{\rho_\infty V_{cc}^2}{2} + \zeta_{out-train} \frac{\rho_s V_{out}^2}{2} + \zeta_{out-B} \frac{\rho_s V_{out}^2}{2} \quad (19b)$$

Substituting Eq. (9), (18), (19), (14), (11) and (3) into Eq. (1), the simplified model of the required driving force at entrance C for the train stopped near the cross-passage during a fire under forced ventilation can be described as follows:

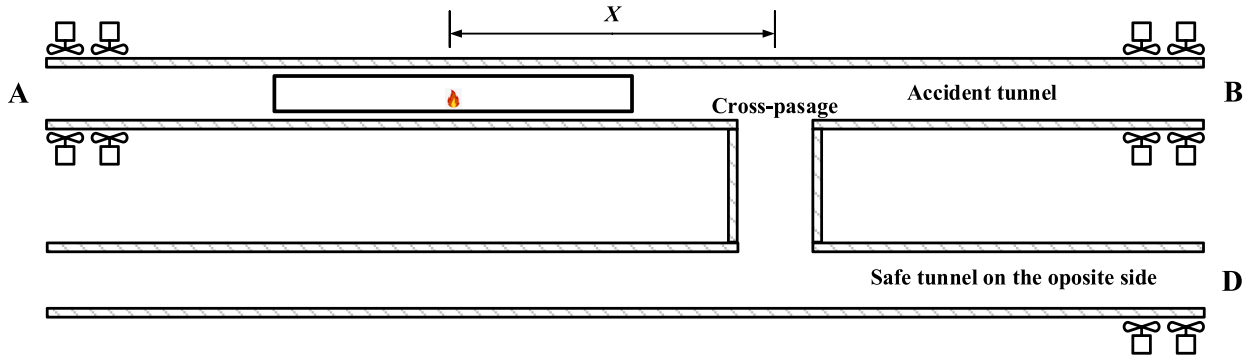


Fig. 4. Schematic diagram of fan layout.

2.3. Type selection of the fan at portal D

In the context of the segment from portal D to portal C, as depicted in Fig. 1, The pressure at cross-section C within the secure tunnel on the opposing side can be expressed as:

$$P_C = P_D - \lambda \frac{L_d}{2 D_t} \rho_\infty V_d^2 \quad (21)$$

Substituting Eq. (21) into Eq. (17) and (20), the expression of the driving force and ventilation velocity necessary for thermal smoke prevention in the opposite side safe tunnel can be deduced as follows:

$$P_D - \lambda \frac{L_d}{2 D_t} \rho_\infty V_d^2 = \left\{ \begin{array}{l} P_A + \left(\zeta_{in-C} + q_\delta^2 \left(\left(\frac{A_t}{A_{cross}} \right)^2 - 2 \right) + 4q_\delta - 1 \right) \frac{\rho_\infty V_{cc}^2}{2} + \lambda \frac{1}{2} \frac{L_d}{D_c} \rho_\infty V_{cc}^2 - \lambda \frac{1}{2} \frac{L_b}{D_t} \rho_\infty \frac{\dot{Q}V_c}{c_p \rho_\infty D_t T_\infty} \\ - \frac{1}{2} \frac{\dot{Q}V_c}{c_p A_t T_\infty} - \lambda \frac{1}{2} \frac{(L_a + L_b)}{D_t} \rho_\infty V_c^2 - \lambda_{train} \frac{1}{2} \frac{(L_{t1} + L_{t2})}{D_t} \rho_\infty V_c^2 - \lambda_{train} \frac{1}{2} \frac{L_{t2}}{D_t} \rho_\infty \frac{\dot{Q}V_c}{c_p \rho_\infty D_t T_\infty} \text{ Train stopped in front of} \\ - [\zeta_{in-A} + \zeta_{in-train} + \zeta_{out-train} + q_\delta(2 - q_\delta)] \frac{\rho_\infty V_c^2}{2} - [q_\delta(2 - q_\delta) + \zeta_{out-train}] \frac{\rho_\infty}{2} \frac{\dot{Q}V_c}{c_p \rho_\infty D_t T_\infty} \text{ the cross - passage} \\ P_A + \left(\zeta_{in-C} + q_\delta^2 \left(\left(\frac{A_t}{A_{cross}} \right)^2 - 2 \right) + 4q_\delta - 1 \right) \frac{\rho_\infty V_{cc}^2}{2} + \lambda \frac{1}{2} \frac{L_d}{D_c} \rho_\infty V_{cc}^2 - \frac{1}{2} \frac{\dot{Q}V_c}{c_p A_t T_\infty} \\ - \lambda \frac{1}{2} \frac{L_a}{D_t} \rho_\infty V_c^2 - \lambda_{train} \frac{1}{2} \frac{(L_{t1} + L_{t2})}{D_t} \rho_\infty V_c^2 - \lambda_{train} \frac{1}{2} \frac{L_{t2}}{D_t} \rho_\infty \frac{\dot{Q}V_c}{c_p \rho_\infty D_t T_\infty} \text{ Train stopped near} \\ - [\zeta_{in-A} + \zeta_{in-train} + q_\delta(2 - q_\delta)] \frac{\rho_\infty V_c^2}{2} - q_\delta(2 - q_\delta) \frac{\rho_\infty}{2} \frac{\dot{Q}V_c}{c_p \rho_\infty D_t T_\infty} \text{ the cross - passage} \end{array} \right. \quad (22)$$

The required driving force to prevent the smoke backflow in the cross-passage is very important parameter for the metro tunnel design

Table 1 Summary of experimental cases.

No.	Fire location X(m)	Fan status	Number of fans
1	120	A: Supply, B: Exhaust, D: Off	A: 4, B: 4, D: 0
2	120	A: Supply, B: Exhaust, D: Supply	A: 3, B: 4, D: 1
3	120	A: Supply, B: Exhaust, D: Supply	A: 2, B: 4, D: 2
4	120	A: Exhaust, B: Supply, D: Off	A: 4, B: 4, D: 0
5	120	A: Exhaust, B: Supply, D: Supply	A: 4, B: 3, D: 1
6	120	A: Exhaust, B: Supply, D: Supply	A: 4, B: 2, D: 2
7	0	A: Exhaust, B: Supply, D: Off	A: 4, B: 4, D: 0
8	0	A: Exhaust, B: Supply, D: Supply	A: 4, B: 3, D: 1
9	0	A: Exhaust, B: Supply, D: Supply	A: 4, B: 2, D: 2

and fan selection. Therefore, Eq. (22) is employed to establish the relationship between the driving force required in the both side tunnels and the ventilation velocity within the cross-passage. In Eq. (22), P_A , V_c , P_D , and V_d represent the supply air parameters of the ventilation fans in the both side tunnels. Some parameters, namely, λ , λ_{train} , $\zeta_{in-train}$, $\zeta_{out-train}$ and V_{cc} , remain unknown. The explicit determination of these parameters will be clarified in the subsequent sections.

It is important to note that this study does not account for conditions where the fire source is located downstream of the tunnel cross-passage. Under critical conditions, as long as the combined airflow in the tunnel cross-passage and the main tunnel exceeds the critical velocity, the smoke will not propagate upstream.

3. Full-scale cold smoke experiment

Full-scale combustion tests incur significant expenses and are constrained by the operational timetable of the subway system. Moreover,

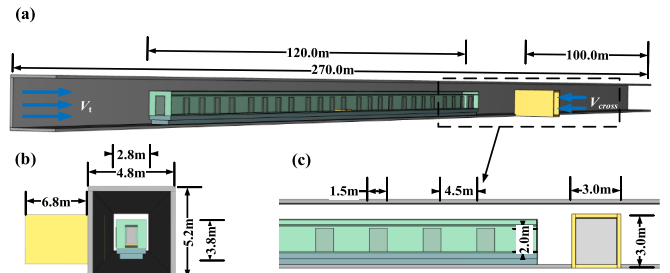


Fig. 5. Schematic of the FDS model.

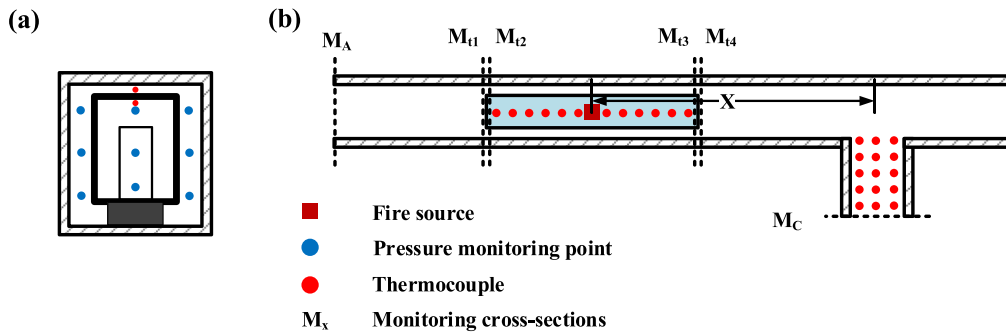


Fig. 6. Schematic of measurement points arrangement.

Table 2
Summary of numerical simulation conditions.

Test no.	HRR Q (MW)	Fire location X (m)	Main tunnel ventilation velocity V_t (m/s)
1 ~ 7	0	100	3.6, 3.8, 4.0, 4.2, 4.4, 4.6, 4.8
8 ~ 127	5,4,3,2	0, 20, 40, 60, 80, 100	3.6, 3.8, 4.0, 4.2, 4.4

replicating and repeating such experiments present inherent difficulties. In place of this, cold smoke experiments were conducted to study smoke dynamics. As a result, full-scale cold smoke verification experiments were carried out in the metro tunnel in Zhengzhou, as depicted in Fig. 3. The dimensions of the tunnel correspond to those of the numerical simulation model. Within the tunnel, a setup of 10 VCF fans allows for adjusting the direction of air supply. Each fan is designed with an air volume of $60 \text{ m}^3/\text{s}$ and the ability to generate a total pressure of 1000 Pa. To illustrate the arrangement of fans the cross-section layout of the ventilation system is presented in Fig. 4. To ensure precise measurement results, a total of 30 measuring points were strategically placed within the tunnel section, with an additional 15 measuring points distributed in the cross-passage section. The ventilation velocity was measured using a hot-wire anemometer with an accuracy of 0.01 m/s. The experimental cases are summarized in Table 1. The comparative results between full-scale cold smoke experimental data and theoretical analysis will be presented in Section 5.1.

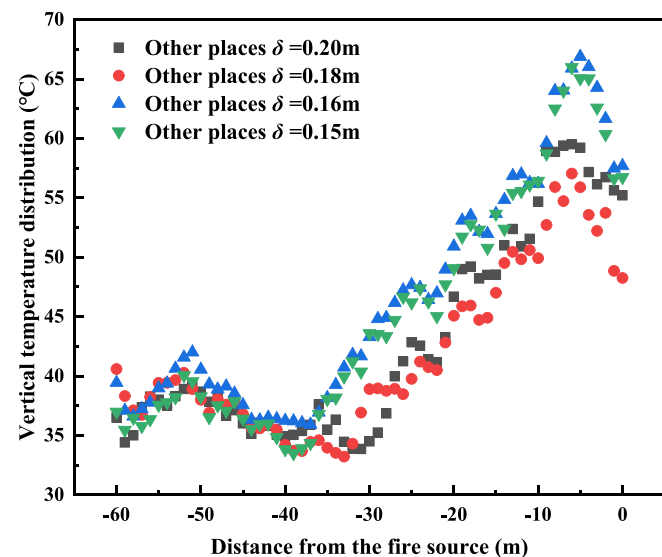


Fig. 7. Vertical temperature distribution beneath the tunnel ceiling under different mesh size under $Q = 5 \text{ MW}$.

4. Numerical simulation

The current study utilized Fire Dynamics Simulator (FDS 6.7.6), a widely employed tool in the field of fire safety. Numerous works have demonstrated its effectiveness in validating metro tunnel fire scenarios (Cong et al., 2022; Ren et al., 2021).

4.1. FDS model

The FDS physical model was established following the actual dimensions of the local metro in Zhengzhou, China. The metro tunnel consists of a main tunnel, an underground train consisting of 6 compartments and a cross-passage is displayed in Fig. 5. The dimension of the full-size main tunnel is 270 m (length) \times 4.8 m (width) \times 5.2 m (height), based on the aspect ratio of real tunnels. Each train carriage dimension is 20 m (length) \times 2.8 m (width) \times 3.8 m (height), and the blocking rate is 0.43. The carriage clear height is 2.2 m, which is from 1 m to 3.2 m above the tunnel ground. Four side doors in each carriage are evenly distributed every 4.5 m along the sidewall. At the same time, two emergency evacuation doors located at the end of the train are set to open, with the same size of 1.2 m (width) \times 2.5 m (height). The cross-passage dimension is 6.8 m (length) \times 3.0 m (width) \times 3.0 m (height), located on the side door opening side 100 m away from the downstream exit. A cuboid fire source is specified as "BURNER" with the dimensions of 2 m (length) \times 1.8 m (width) \times 0.2 m (height). The

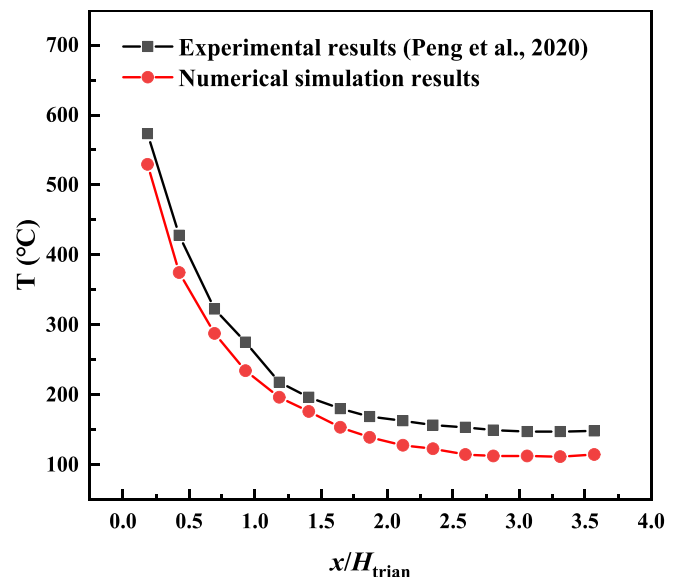


Fig. 8. The comparison of the train ceiling temperature distribution between simulation and experiments.

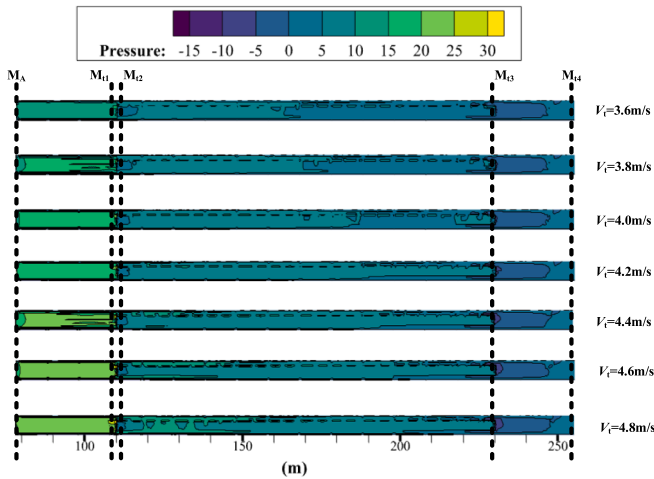


Fig. 9. Pressure parameter slice nephograms with different longitudinal ventilation velocities.

thickness of the tunnel and train carriage are set to 0.3 m and 0.1 m respectively. The materials of tunnel surfaces are specified as concrete, with conductivity, specific heat, and density being 1.80 W/(m·k), 1.04 KJ/(kg·k), 2280 kg/m³, respectively. The materials of the train carriage surfaces are specified as steel, and the corresponding parameters are 45.8 W/(m·k), 0.46 KJ/(kg·k), 7850 kg/m³. The tunnel portal and cross-passage portal are set as “SUPPLY” to accomplish uniform air supply velocity for the cross section. The tunnel exit is set as “OPEN”.

The subway train may stop in interval tunnel due to power system of the train failures after the accident (Cong et al., 2022). This study focuses on luggage-induced fire scenarios within train carriages. Since the 2012 release of “Fire Protection Requirements for Urban Rail Transit Vehicles-China (CJ/T 416-2012)”, there’s a growing trend in using fire-resistant materials in metro carriages. Experimental findings suggest that, in controlled fire situations within metro carriages, an HRR of 5 MW can be considered a critical point. For scenarios involving uncontrolled combustion throughout the entire carriage, a maximum HRR of 11 MW is recommended (Shi et al., 2020). Assuming fire containment within the carriage, this study considers a maximum HRR of 5 MW for luggage-induced carriage fires. Four fire sizes (2 MW, 3 MW, 4 MW, 5 MW) are selected to represent the unfavorable scenarios (Su et al., 2023). The fire source position (X) is the distance of fire and supply air flow portal of the cross-passage, six different fire positions (0 m, 20 m, 40 m, 60 m, 80 m, 100 m) are considered in this study, and the position of fire source changes with the movement of train position. Fig. 6 shows the scheme of measurement points arrangement in the FDS model. Four pressure monitoring cross-sections are used to monitor the portal total pressure (M_A, M_C), pressure losses induced by the tunnel and train wall friction (M₁₂ ~ M₁₃) and pressure losses induced by the train local resistance (M₁₁ ~ M₁₂, M₁₃ ~ M₁₄) respectively. Among them, nine pressure measurement points are evenly placed on each cross-section to

Table 3

The refined analytical treatment of pressure loss in each region.

Energy loss coefficient	Measuring section	Fitting formulas
λ	M _A ~ M ₁₁	$P_{M_A} - P_{M_{11}} = \lambda \frac{1}{2} \frac{L_{M_A-M_{11}}}{D_t} \rho_{\infty} V_t^2$
$\zeta_{in-train}$	M ₁₁ ~ M ₁₂	$P_{M_{11}} - P_{M_{12}} = \zeta_{in-train} \frac{\rho_{\infty} V_t^2}{2}$
λ_{train}	M ₁₂ ~ M ₁₃	$P_{M_{12}} - P_{M_{13}} = \lambda_{train} \frac{1}{2} \frac{L_{M_{12}-M_{13}}}{D_t} \rho_{\infty} V_t^2$
$\zeta_{out-train}$	M ₁₃ ~ M ₁₄	$P_{M_{13}} - P_{M_{14}} = \zeta_{out-train} \frac{\rho_{\infty} V_t^2}{2} + \lambda \frac{1}{2} \frac{L_{M_{13}-M_{14}}}{D_t} \rho_{\infty} V_t^2$

obtain the average pressure of the cross-section. The distances between the monitoring section (M₁₁~M₁₄) and the train boundary are all 0.1 m. 20 thermocouples are placed 0.1 m beneath the tunnel ceiling along the cross-passage to ensure that smoke will not overflow into the cross-passage. At the same time, 60 thermocouples are placed 0.1 m beneath the train ceiling with the interval of 2 m and 60 thermocouples are placed 0.1 m beneath the tunnel ceiling with the interval of 2 m to ensure that smoke will not diffuse upstream. The total information of specific tests was summarized in Table 2. For the effect of train blockage and main tunnel ventilation velocity on the energy loss coefficient, seven main tunnel ventilation velocities are considered from test 1 to 7 under non-fire condition. At the same time, the cross-passage ventilation velocities in these conditions are set to 0 m/s. Test 8 to 127 presents a series of conditions to obtain the critical cross-passage ventilation velocity with different fire location, heat release rate and main tunnel ventilation velocity. It is worth noting that in this study the variation of the longitudinal ventilation velocity in main tunnel is under the critical condition (Su et al., 2023). In the scenario of a fire occurring in the middle of the carriage, the minimum critical ventilation velocity for a fire with a heat release rate of 5 MW was determined to be 3.6 m/s for the main tunnel. The ambient temperature is 20 °C and the environmental pressure is 101 kPa. The simulation time is set to be 700 s to ensure that the smoke movement is in a steady spread state.

4.2. Grid system

Grid size plays a vital role in numerical simulations as it directly affects the accuracy of calculations. The characteristic fire diameter is a pivotal parameter for identifying the optimal grid size. The characteristic fire diameter to the grid size, denoted as D^*/δ_x , is a significant criterion for evaluating mesh resolution, where δ_x is the grid size. Mcgrattan et al. (2017) proposed that the appropriate range for the value of D^*/δ_x is between 4 and 16, which can be expressed as:

$$D^* = \left(\frac{Q}{\rho_a C_p T_a g^{1/2}} \right)^{2/5} \quad (23)$$

Considering the heat release rate values in this work, it is suggested that the grid sizes ranged from 0.125 m ~ 0.20 m to enhance the applicability of the grid size. Therefore, the mesh size 5 m from the fire center in both direction is set to be 0.125 m. At the same time, except for the fire center, the mesh size setting range is 0.15 m to 0.20 m in other places. In this study, mesh size sensitivity analysis of the FDS prediction have also conducted. Four grid systems have been considered, with the number of mesh increases from 1,578,000 to 3,598,000. Fig. 7 shows a typical comparison of four grid systems for the vertical temperature distribution under natural ventilation when the HRR is 5 MW. 60 temperature measurement points in the area 60 m downstream of the fire source were compared. It was shown that there is no significant difference of vertical temperature distribution between two mesh systems ($\delta = 0.16$ m and $\delta = 0.15$ m). Considering saving resources, the mesh size in other places is set to be 0.16 m with the number of mesh.

4.3. Model validation

To validate the efficacy of the FDS model, a comparison was conducted between the simulation data and the experimental results (Peng et al., 2020). The train fire experiments occurred within a 1:5 reduced-scale train model measuring 4.0 m in length, 0.55 m in width, and 0.42 m in height. The numerical model employed a grid size of $\delta = 0.16$ m in other places, resulting in a total of 2,935,000 grid elements. Fig. 8 illustrated the comparison of experimental and numerical results on the dimensionless longitudinal train ceiling temperature distribution. It was observed that the numerical simulation aligned with the temperature distribution observed in the experiments, although there was some discrepancy, with a maximum deviation of 37 °C, falling within a margin

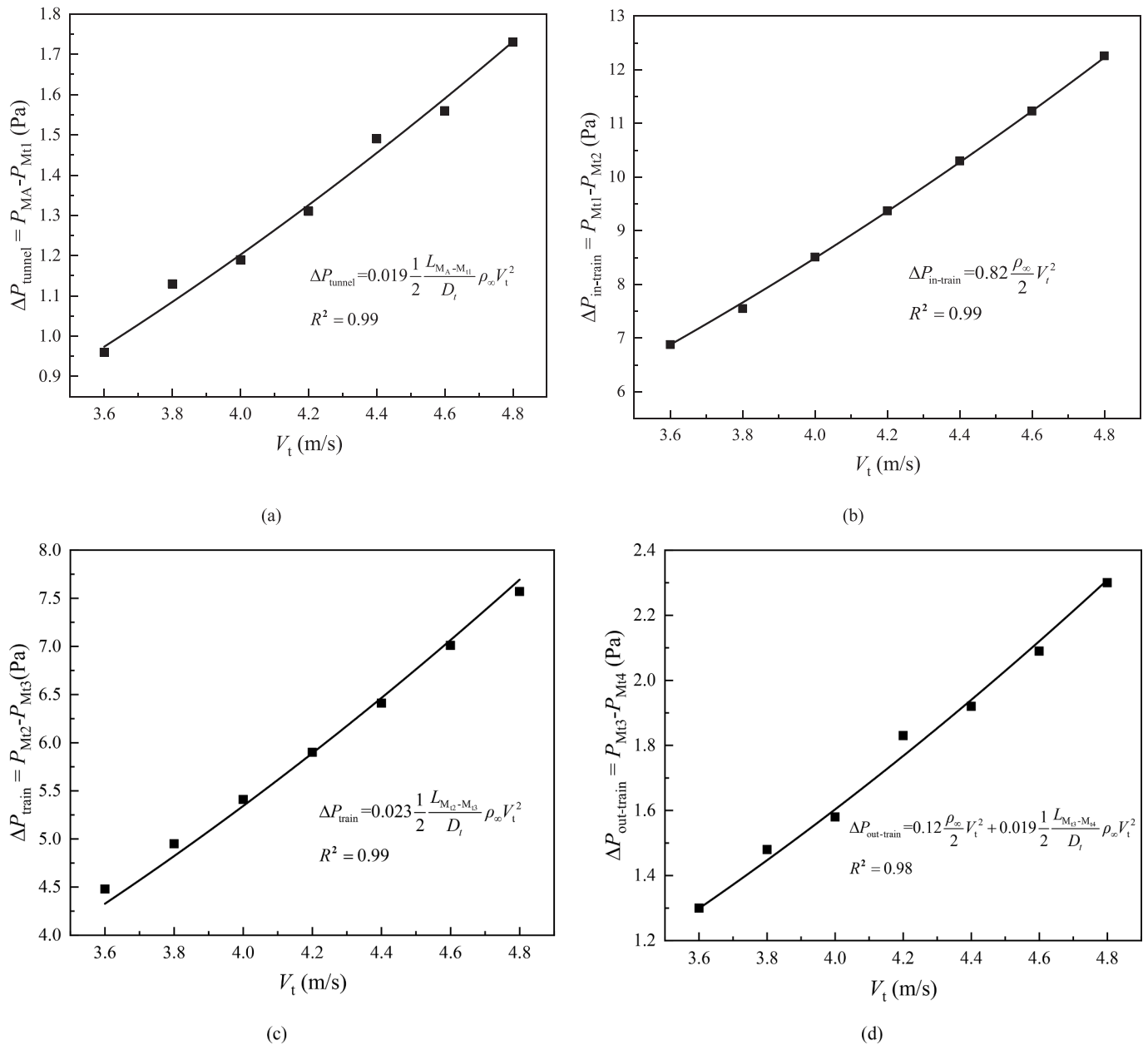


Fig. 10. The variation of pressure loss with longitudinal ventilation velocity: (a) $M_A \sim M_{t1}$, (b) $M_{t1} \sim M_{t2}$, (c) $M_{t2} \sim M_{t3}$, (d) $M_{t3} \sim M_{t4}$.

of error of 10 %. This was because, with the emergency evacuation doors open, the smoke accumulation in the carriage was reduced. However, this aspect was not considered during the experiments. Overall, the ceiling temperature in simulations followed an exponential decay pattern as it diffused, closely mirroring the experimental findings. Therefore, the model used in this study was deemed feasible.

5. Results and discussion

5.1. Energy loss coefficient

Fig. 9 shows the pressure fields at steady period of airflow movement without fire, in which the image is a horizontal cross-sectional image at a height of 2.5 m. Therein, metro train divides main tunnel into upstream region, metro region and downstream region. In order to better show the results, the downstream length in Fig. 9 only shows the pressure distribution within 25 m. Attributed to train blockage, the longitudinal airflow is blocked at the front of the train, which causes to a

pressure drops sharply in this region. In metro region, the airflow in the train carriage and tunnel is complicated induced by the coupling effect of side doors. In general, the pressure gradually decreases along the train, but the resistance along the train is not significant compared with the tunnel. Moreover, it is obvious to see that a negative pressure zone is formed at the rear of the train induced by train blockage, downstream negative pressure length is related to longitudinal ventilation velocity but remains relatively stable. As the longitudinal velocity increases from 3.6 m/s to 4.8 m/s, it can be observed that the length of the negative pressure zone measures approximately 20 m. These phenomena probably indicate that the measurement of local resistance of airflow exiting the train is restricted by the negative pressure zone. As a result, to ensure a uniform pressure distribution across the section, the measurement of local resistance of airflow exiting the train involved shifting M_{t4} backward by 25 m.

The relationship between pressure loss and longitudinal velocity exhibits a quadratic function correlation. The precise fitting formulas governing the pressure loss in each distinct region have been

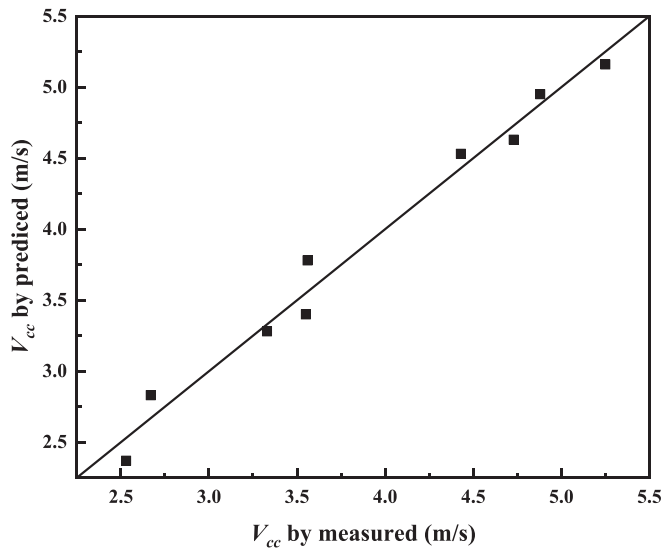


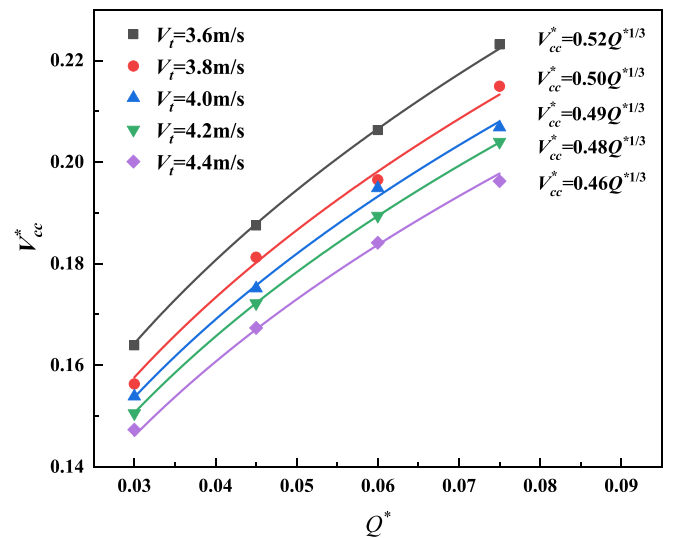
Fig. 11. Comparison of velocity in the cross-passage between predictions and experimental results.

meticulously elucidated in Table 3, exemplifying the refined analytical treatment employed in this study. Fig. 10 unveils the fitting outcomes of pressure loss varying with longitudinal ventilation velocities for each region, exhibiting an exceptional degree of conformity with their respective formulas, all surpassing 0.98. The obtained results stand as follows: $\lambda = 0.019$, $\zeta_{in-train} = 0.82$, $\lambda_{train} = 0.023$ and $\zeta_{out-train} = 0.12$. It is worth noting that, the local resistance coefficient of the train front is much larger than that of the rear with a difference of 0.7. This segment of resistance assumes paramount significance in the meticulous evaluation of overall resistance loss. Furthermore, the results derived from numerical simulations reveal a remarkable resistance coefficient of $\lambda = 0.019$ along the tunnel. Notably, this finding closely aligns with the guidelines for tunnel design of 0.02, further solidifying the credibility and feasibility of the employed numerical simulation methodology (Transport, 2014; Yan et al., 2020).

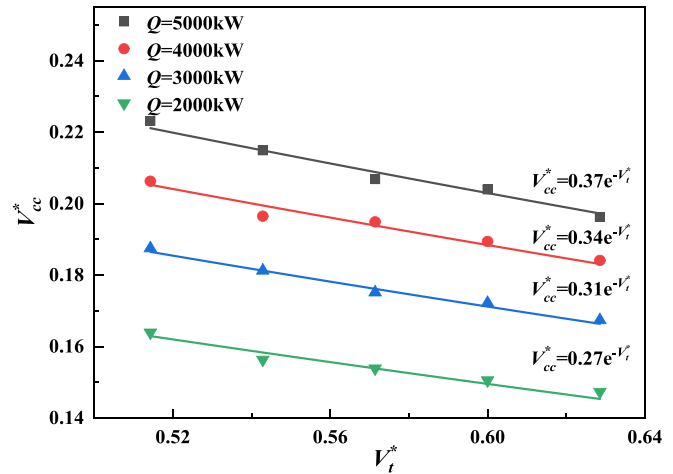
Therefore, the reliability of Eq. (22) can be verified through full-scale cold smoke experiment, building upon the existing parameters. It is worth noting that, it is not feasible to control the total pressure and flow rate of the fan due to constraints in experimental conditions. Hence, the feasibility of Eq. (22) is verified by measuring the velocity in the cross-passage under the given experimental conditions. At the same time, it is not necessary to consider the resistance loss caused by thermal expansion in the cold smoke experiment. Substituting P_A , P_D , V_C , V_D , λ , λ_{train} , $\zeta_{in-train}$ and $\zeta_{out-train}$ into Eq. (22), the velocity in the cross-passage V_{cc} can be calculated. The velocities in cross-passage obtained from Eq. (22) have been contrasted with experimental results, as shown in Fig. 11. The small variance between the predicted velocities and the actual experimental results is evident. This signifies the viability of the method, which relies on tunnel pressure balance for analyzing critical ventilation within the cross-passage.

5.2. Critical velocity and required driving force in the cross-passage

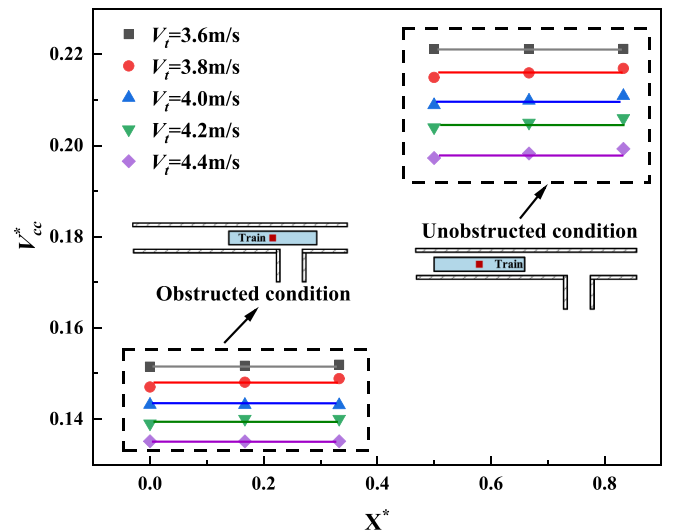
The critical velocity in the cross-passage (V_{cc}) can be ascertained through dimensionless analysis, subsequently enabling the acquisition of the corresponding critical supply parameters via the application of Eq. (22). The critical velocity in the cross-passage (V_{cc}) is affected by the heat release rate (Q), train length (L_{train}), longitudinal ventilation velocity (V_t), fire location (X), hydraulic diameter of the tunnel (D_t), hydraulic diameter of the cross-passage (D_{cross}), air density (ρ_{∞}), ambient temperature (T_{∞}), thermal capacity of air (c_p), and gravitational acceleration (g). The elucidation of the critical velocity function for smoke



(a)



(b)



(c)

Fig. 12. Effect of various factors on critical velocity in the cross-passage: (a) Effect of Q^* on V_{cc}^* at a fire source location of 60 m, (b) Effect of V_t^* on V_{cc}^* at a fire source location of 60 m, (c) Effect of X^* on V_{cc}^* at a heat release rate of 5 MW.

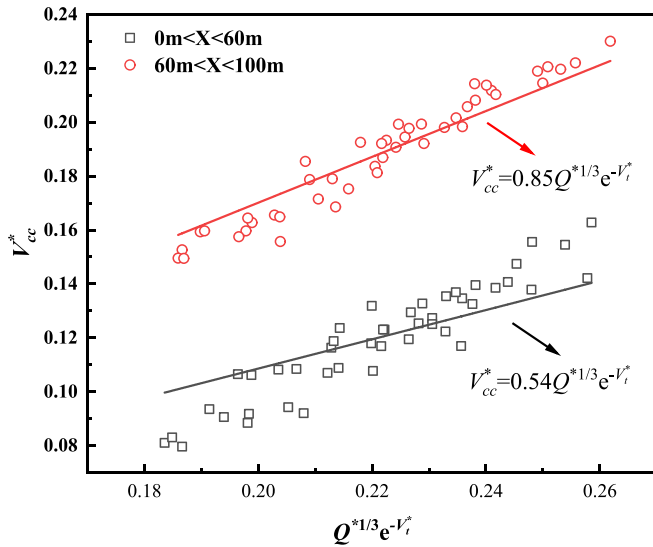


Fig. 13. Relationship between V_{cc}^* and $Q^{1/3}\exp(-V_t^*)$ with various fire locations.

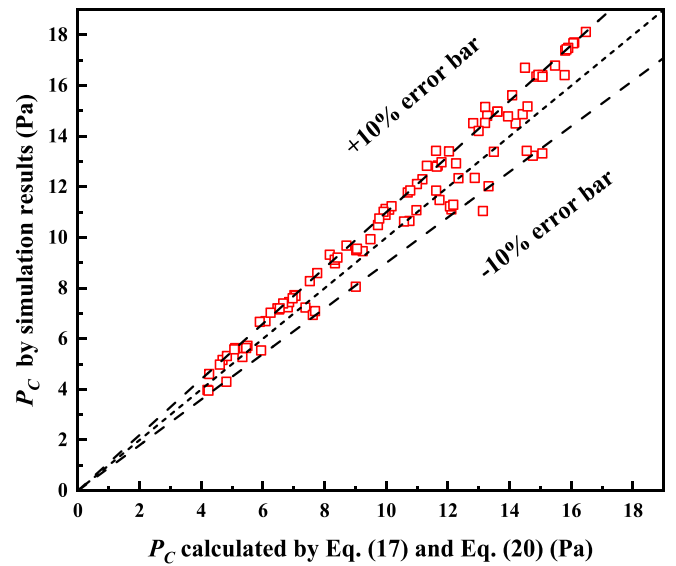


Fig. 15. Comparison of theoretical model-predicted values and simulation values.

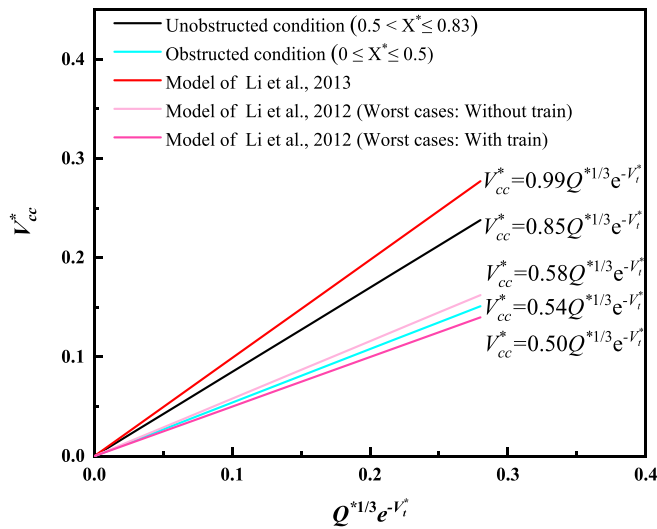


Fig. 14. Comparison between current model (Eq. (28)) and Li's model.

control in a tunnel cross-passage is presented as follows:

$$f(V_{cc}, D_t, Q, V_t, D_{cross}, L_{train}, c_p, \rho_\infty, T_\infty, g, X) = 0 \quad (24)$$

According to Ji et al. (2012), the variables devoid of interdependence constitute the independent variables under investigation. Thus, Eq. (24) can be reconfigured in the subsequent manner:

$$f\left(\frac{V_{cc}^2}{gD_{cross}}, \frac{Q}{\rho_\infty c_p T_\infty g^{1/2} D_t^{5/2}}, \frac{V_t^2}{gD_t}, \frac{X}{L_{train}}\right) = 0 \quad (25)$$

Hence, Eq. (25) can be reformulated into a more comprehensive expression:

$$V_{cc}^* = f(Q_t^*, V_t^*, X^*) \quad (26)$$

where $V_{cc}^* = V_{cc}/\sqrt{gD_{cross}}$ is dimensionless critical ventilation velocity in the cross-passage, $V_t^* = V_t/\sqrt{gD_t}$ is the dimensionless longitudinal ventilation velocity in the tunnel, $X^* = X/L_{train}$ is the dimensionless fire location. Fig. 12(a) depicts the influence of heat release rate on the critical velocity in a tunnel cross-passage. The results were derived through numerical simulations involving the fire located 60 m away

from the cross-passage, encompassing tunnel ventilation velocities ranging from 3.6 m/s to 4.4 m/s. Evidently, the critical velocity in a tunnel cross-passage escalates proportionally with the heat release rate, exhibiting a variation governed by a dimensionless heat release rate exponent following a power law of 1/3. Fig. 12(b) illustrates the impact of tunnel ventilation velocity on critical velocity in the cross-passage. Notably, critical velocity exhibits an inverse relationship with tunnel ventilation velocity. Additionally, the experimental data appears to align well with a natural exponential function of tunnel ventilation velocity. It is worth noting that the congruence of their association resonates of the associations depicted in Fig. 12(a) and Fig. 12(b) aligns exceptionally well with prior scholarly discoveries (Li et al., 2013). Fig. 12(c) shows the effect of the fire source location on critical velocity in the tunnel cross-passage. It is imperative to underscore that the fire source location varies in accordance with the train position. Evidently, the data illustrates that the critical velocity in the cross-passage under unobstructed conditions surpasses that of the blocking scenario. The rationale behind this lies in the train obstruction, which augments the flow velocity in the vicinity. This, in turn, induces a reduction in pressure, resulting in a decrease in the inertial force that the cross-passage must furnish. At the same time, it was found that the position of the fire source exhibited limited influence on the critical velocity in the cross-passage under these two conditions. Hence, the influence of the fire source location on the critical velocity in the cross-passage can be respectively disregarded in both scenarios.

Drawing from the preceding analysis of the impacts stemming from distinct parameters on the critical velocity, it is evident that the dimensionless critical velocity exhibits a variation following a power law of 1/3 with respect to the dimensionless heat release rate, and conforms to an exponential relationship with tunnel ventilation velocity. Subsequently, Eq. (26) for both obstructed and unobstructed conditions can be reformulated as follows:

$$V_{cc}^* = CQ^{1/3}e^{-V_t^*} \quad (27)$$

Fig. 13 depicts the outcomes of the critical velocity in the cross-passage, considering different fire heat release rates, longitudinal ventilation velocities and fire locations. Notably, all simulation data demonstrate an alignment with the subsequent equation:

$$V_{cc}^* = \begin{cases} 0.85Q^{*1/3}e^{-V_i^*} & \text{Unobstructed condition } (0.50 < X^* \leq 0.83) \\ 0.54Q^{*1/3}e^{-V_i^*} & \text{Obstructed condition } (0 < X^* \leq 0.33) \end{cases} \quad (28)$$

This study compared the critical velocities in the metro tunnel cross-passage with prediction models for conventional single tunnels (Li et al., 2013) and long railway tunnels (Li et al., 2012), as shown in Fig. 14. In the context of conventional tunnels, this study shares similarities with Li's research as both investigations encompass factors such as heat release rate, fire source location, and longitudinal ventilation velocity (Li et al., 2013). These considerations yielded comparable patterns to the results of the present study, albeit without addressing the influence of train blockage. The outcomes reveal a consistent trend where the predictions generated by the current study's model consistently remain lower than those of Li's model. This discrepancy can be attributed to the influence of train blockage. In unobstructed conditions, due to the fact that the farthest considered fire source location in this study is only 100 m away, the airflow does not attain uniformity when passing through the cross-passage. This disparity causes the velocity passing through the cross-passage to exceed the average velocity, leading to a localized reduction in instantaneous pressure and consequently resulting in a decrease in the required critical velocity in the cross-passage.

For long railway tunnels, Li et al. (2012) investigated the critical velocity in cross-passages under natural ventilation conditions ($V_t = 0$ m/s) in the main tunnel. Considerations encompassed factors such as train blockage, fire source location, cross-passage opening height, and the combination of multiple cross-passages supplying air. Results indicated that the most unfavorable scenario occurred when the fire source was positioned directly in front of the cross-passage ($X^*=0$), with an opening height of 85 mm. Simultaneously, the critical velocity induced by train blockage was 0.86 times smaller compared to the unblocked condition. Diverging from Li's model, the present study focused solely on a single cross-passage, with all train doors assumed to be open. This choice mitigates the impact on airflow around the train relative to a scenario with closed doors. Fig. 14 illustrates that, in Li's study, the most unfavorable scenario closely aligns with our current study's obstructed condition, attributed to the open doors in our model. In contrast to open doors, closed doors would elevate wind speeds around the train, increasing the pressure difference between the cross-passage and the main tunnel and subsequently reducing the critical velocity requirement in the connecting passage.

Under critical conditions, the required driving force for portal C was summarized from the outcomes of numerical simulations. At the same time, the predictions of the driving force at portal C calculated by Eq. (22) are compared with simulation results, as shown in Fig. 15. It can be seen the predicted values are in good agreement with simulation results, indicating that Eq. (22) can predict the total pressure at portal C induced by train fires in metro tunnel with cross-passage for given fire heat release rates, longitudinal ventilation velocities, fire locations and critical velocities in the cross-passage within a margined error of 10 %.

6. Conclusions

This study explores the feasibility of eliminating fireproof doors in future metro tunnels. Theoretical analysis of pressure losses in metro tunnel fire is conducted to investigate the critical velocity and the required driving force in the tunnel cross-passage. Simultaneously, the type selection of fan in the opposite side safe tunnel for preventing the diffusion of smoke to the safe tunnel is investigated, with the aim of proposing the removal of fireproof doors in cross-passages. The major conclusions are as follows:

1. Theoretical analysis prove that the local resistance for metro tunnel is a significant factor which results in the smoke control law is different with single tunnel. The train location effect the frictional

resistance and local resistance induced by cross-passage. The theoretical models of the required driving force in the metro tunnel cross-passage for different train locations are obtained.

2. The energy loss coefficients induced by trains are obtained. At the same time, full-scale cold smoke experimental work was conducted to investigate the effect of fan supply parameters of opposite tunnel on the velocity of the cross-passage. Theoretical models provided reasonable results for estimating the pressure loss caused by metro train. The predictions are in good agreement with the experimental data.
3. The theoretical model on the basis of the dimensionless analysis in metro tunnel cross-passage is proposed to predict the critical velocity in the cross-passage under the different cases of the train location. The required driving force at cross-passage entrance is obtained which is closed to the simulated value.

In summary, the recommendation to eliminate tunnel fireproof doors is deemed feasible by optimizing the airflow parameters for fans on both sides of the tunnel. This optimization ensures that the cross-passages attain the critical velocity conditions necessary for safe ventilation. It should be noted that the location of the train fire only considered within 100 m from the cross-passage. Obvious differences in the motion characteristics of thermal smoke become inevitably apparent when the train is far from the cross-passage. In these scenarios, the applicability of above correlations requires additional validation. Concurrently, it is essential to note that the existing model lacks continuity. During the transition of the train from a blocked to an unblocked condition, the critical ventilation velocity within the cross-passage should demonstrate a continuous increment. Future investigations will involve a thorough analysis of the influence of additional fire source positions on this phenomenon. Furthermore, the current model maintains a fixed scale (e. g., with the cross-passage dimensions at 6.8 m × 3.0 m × 3.0 m). Future research should also investigate and verify the potential influence of cross-passage dimensions.

CRediT authorship contribution statement

Zhihe Su: Investigation, Methodology, Writing – original draft. **Yanfeng Li:** Conceptualization, Funding acquisition, Supervision. **Hua Zhong:** Writing – review & editing. **Junmei Li:** Supervision, Writing – review & editing. **Zhicheng Guo:** Investigation, Software. **Xin Yang:** Investigation. **Shi Yang:** Software.

Declaration of competing interest

The authors declare that they have no known competing financial interests or personal relationships that could have appeared to influence the work reported in this paper.

Data availability

Data will be made available on request.

Acknowledgements

This work was supported by the Beijing Natural Science Foundation (Grant No: 8222002) and the Natural Science Foundation of China (Grant No: 51378040). We sincerely appreciate this support.

References

- Chen, C., Jiao, W., Zhang, Y., Shi, C., Lei, P., Fan, C., 2023a. Experimental investigation on the influence of longitudinal fire location on critical velocity in a T-shaped tunnel fire. *Tunn. Undergr. Space Technol.* 134, 104983.
- Chen, C., Lu, T., Zhang, Y., Shi, C., Jiao, W., 2023b. Experimental study on temperature profile and critical velocity in bifurcated tunnel fire with inclined transverse cross-passage. *Int. J. Therm. Sci.* 186, 108120.

- Cong, W., Shi, L., Shi, Z., Peng, M., Yang, H., Zhang, S., Cheng, X., 2020. Effect of train fire location on maximum smoke temperature beneath the subway tunnel ceiling. *Tunn. Undergr. Space Technol.* 97, 103282.
- Cong, W., Shi, L., Shi, Z.C., Peng, M., Yang, H., Cheng, X.D., 2022. Numerical study on the ceiling gas temperature in a subway train with different fire locations. *Build. Simul.* 15, 549–560.
- Du, T., Yang, D., Ding, Y., 2018. Driving force for preventing smoke backlayering in downhill tunnel fires using forced longitudinal ventilation. *Tunn. Undergr. Space Technol.* 79, 76–82.
- Feng, S., Li, Y., Hou, Y., Li, J., Huang, Y., 2020. Study on the critical velocity for smoke control in a subway tunnel cross-passage. *Tunn. Undergr. Space Technol.* 97, 103234.
- Gao, Z., Li, L., Sun, C., Zhong, W., Yan, C., 2022. Effect of longitudinal slope on the smoke propagation and ceiling temperature characterization in sloping tunnel fires under natural ventilation. *Tunn. Undergr. Space Technol.* 123, 104396.
- Hager, W.H., 2010. *Wastewater Hydraulics: Theory and Practice*. Springer, Heidelberg Dordrecht London New York.
- Hu, P., Zhang, Z., Zhang, X., Tang, F., 2020. An experimental study on the transition velocity and smoke back-layering length induced by carriage fire in a ventilated tunnel. *Tunn. Undergr. Space Technol.* 106, 103609.
- Huang, Y., Li, Y., Li, J., Li, J., Wu, K., Zhu, K., Li, H., 2020. Modelling and experimental investigation of critical velocity and driving force for preventing smoke backlayering in a branched tunnel fire. *Tunn. Undergr. Space Technol.* 99, 103388.
- Ji, J., Gao, Z.H., Fan, C.G., Zhong, W., Sun, J.H., 2012. A study of the effect of plug-holing and boundary layer separation on natural ventilation with vertical shaft in urban road tunnel fires. *Int. J. Heat Mass Transfer* 55, 6032–6041.
- Jiang, L., Xiao, M., 2022. Effect of tunnel slope on the critical velocity of densimetric plumes and fire plumes in ventilated tunnels. *Tunn. Undergr. Space Technol.* 123, 104394.
- Li, Y.Z., Ingason, H., 2017. Effect of cross section on critical velocity in longitudinally ventilated tunnel fires. *Fire Saf. J.* 91, 303–311.
- Li, Y.Z., Lei, B., Ingason, H., 2010. Study of critical velocity and backlayering length in longitudinally ventilated tunnel fires. *Fire Saf. J.* 45, 361–370.
- Li, Y.Z., Lei, B., Ingason, H., 2012. Scale modeling and numerical simulation of smoke control for rescue stations in long railway tunnels. *J. Fire. Prot. Eng.* 22, 101–131.
- Li, Y.Z., Lei, B., Ingason, H., 2013. Theoretical and experimental study of critical velocity for smoke control in a tunnel cross-passage. *Fire Technol.* 49, 435–449.
- Liu, C., Zhong, M., Song, S., Xia, F., Tian, X., Yang, Y., Long, Z., 2020. Experimental and numerical study on critical ventilation velocity for confining fire smoke in metro connected tunnel. *Tunn. Undergr. Space Technol.* 97, 103296.
- Lu, X., Weng, M., Liu, F., Wang, F., Han, J., Chipok, C., 2022. Effect of bifurcation angle and fire location on smoke temperature profile in longitudinal ventilated bifurcated tunnel fires. *Tunn. Undergr. Space Technol.* 127, 104610.
- Mcgrattan, K.B., Mcdermott, R.J., Weinschenk, C.G., Forney, G.P., 2017. *Fire Dynamics Simulator Users Guide*, 6th edn. National Institute of Standards and Technology, Gaithersburg, MD, USA.
- Peng, M., Cheng, X., Cong, W., Yuen, R., 2020. Experimental investigation on temperature profiles at ceiling and door of Subway carriage fire. *Fire Technol.* 57, 439–459.
- Ren, F., Shi, C., Li, J., Che, H., Xu, X., 2021. Numerical study on the flow characteristics and smoke temperature evolution under double fires condition with a metro train in tunnel. *Tunn. Undergr. Space Technol.* 114, 103943.
- Shi, C.L., Zhong, M.H., Chen, C.K., Jiao, W.B., Li, J., Zhang, Y.L., Zhang, L., Li, Y., He, L., 2020. Metro train carriage combustion behaviors - Full-scale experiment study. *Tunn. Undergr. Space Technol.* 104, 103544.
- Su, Z., Li, Y., Feng, S., Zhong, H., Li, J., Liu, W., Chen, C., Li, J., 2023. A study of the critical velocity and the confinement velocity of fire accident in a longitudinally ventilated underground train with different door opening scenarios. *Tunn. Undergr. Space Technol.* 131, 104776.
- Tang, W., Hu, L.H., Chen, L.F., 2013. Effect of blockage-fire distance on buoyancy driven back-layering length and critical velocity in a tunnel: An experimental investigation and global correlations. *Appl. Therm. Eng.* 60, 7–14.
- Thomas, P.H., 1958. The movement of buoyant fluid against a stream and the venting of underground fires. *Fire Saf. Sci.* 351, 1–9.
- Transport, M.o., 2014. *Guidelines for Design of Ventilation of Highway Tunnels (JTG/T D70/2-02-2014)*. China Communications Press, China.
- Weng, M.-C., Lu, X.-L., Liu, F., Shi, X.-P., Yu, L.-X., 2015. Prediction of backlayering length and critical velocity in metro tunnel fires. *Tunn. Undergr. Space Technol.* 47, 64–72.
- Weng, M.-C., Lu, X.-L., Liu, F., Du, C.-X., 2016. Study on the critical velocity in a sloping tunnel fire under longitudinal ventilation. *Appl. Therm. Eng.* 94, 422–434.
- Wu, Y., Bakar, M.Z.A., 2000. Control of smoke flow in tunnel fires using longitudinal ventilation systems – a study of the critical velocity. *Fire Safety J.* 35, 363–390.
- Yan, X., Li, J., Ye, X., Zeng, Y., Fang, Y., Bai, Y., 2020. Field test and numerical simulation study on energy loss coefficient of vehicle cross-passage area in twin-tunnels. *Tunn. Undergr. Space Technol.* 106, 103572.
- Yao, Y., Qu, B., Zhu, H., Wang, J., Zhao, S., Wang, Q., 2022. Theoretical and numerical study on critical velocity and driving force for preventing smoke backlayering in a connection roadway fire of coal mines. *Tunn. Undergr. Space Technol.* 127, 104566.
- Yao, Y., Wang, R., Xia, Z., Shi, C., Ren, F., 2023. Smoke movement and control in longitudinal ventilated tunnel fires with cross-passages. *Case Stud. Therm. Eng.* 45, 102945.
- Zhang, S., Yao, Y., Zhu, K., Li, K., Zhang, R., Lu, S., Cheng, X.J.T., 2016. Prediction of smoke back-layering length under different longitudinal ventilations in the subway tunnel with metro train. *Tunn. Undergr. Space Technol.* 53, 13–21.
- Zhao, S., Liu, F., Wang, F., Weng, M., Zeng, Z., 2018. A numerical study on smoke movement in a metro tunnel with a non-axisymmetric cross-section. *Tunn. Undergr. Space Technol.* 73, 187–202.